Improving the Morphological and Optical Properties of the $CsPbBr_3$ Films by PbI_2 Substitution for Efficient All-inorganic Perovskite Solar Cells

Fei ZHAO [1] *, Yannan ZHANG [1], Yixin GUO [2]

[1] *School of Photoelectric Engineering, Changzhou Institute of Technology, Changzhou, Jiangsu, 213032, China*
[2] *Department of Physics, Shanghai Normal University, Shanghai 200233, China*

http://doi.org/10.5755/j02.ms.39805

Received 16 December 2024; accepted 13 February 2025

Wide band gap $CsPbBr_3$ perovskite solar cells are becoming one of the ideal candidates for top cells in tandem solar cells. Nevertheless, the defects in $CsPbBr_3$ film prepared by solution deposition method restrict the optoelectronic performance of perovskite solar cells. To solve this problem, a strategy of doping a trace amount of PbI_2 into $CsPbBr_3$ film synthesized by solution deposition is adopted, effectively increasing the average grain size of $CsPbBr_3$ film, decreasing its optical band gap, number of surface grain boundary defects and carrier recombination probability. Simultaneously, the PbI_2-doped $CsPbBr_3$ perovskite solar cells have been successfully prepared. The best conversion efficiency of the $CsPbBr_3$ cells with doping PbI_2 is 6.46 %, which is higher than the efficiency of the undoped $CsPbBr_3$ devices (5.00 %). This study offers a method for manufacturing highly efficient all-inorganic perovskite solar cells.
Keywords: doping PbI_2, $CsPbBr_3$, all-inorganic perovskite solar cells, optical band gap.

1. INTRODUCTION

Organic-inorganic hybrid perovskite solar cell (OIHPSC) has become one of the fastest developing photovoltaic technologies due to their comprehensive advantages such as high performance, low cost and solution processability [1 – 4]. The photoelectric conversion efficiency (PCE) of laboratory-scale organic-inorganic hybrid perovskite devices has increased from 3.8 % to 26 % [5], which is comparable to the efficiency of crystalline-silicon solar cells [6]. Nevertheless, they faces poor moisture, heat, and light stability [7, 8]. To address the aforementioned problems, all-inorganic perovskites ($CsPbI_3$, $CsPbBr_3$, $CsPbIBr_2$ and $CsPbI_2Br$) have been successfully synthesized [9 – 11]. Among these perovskites, the $CsPbBr_3$ based on a wide band gap (~2.3 eV) has attracted a lot of attention owing to its extraordinary humidity and thermal stability [12 – 14]. The advanced $CsPbBr_3$ cell displays an architecture of FTO/Nb_2O_5/$CsPbBr_3$/Carbon. Compared with the OIHPSC device, it significantly simplifies the manufacturing process and reduces costs [15]. Thus, more efforts are being made to enhance the efficiency of carbon-based $CsPbBr_3$ cell without sacrificing its stability.

The $CsPbBr_3$ film based on large grain size and low carrier recombination probability is a key factor for enhancing the efficiency of corresponding cell [16, 17]. Thus, the preparation of $CsPbBr_3$ film with large grain size and low carrier recombination probability is a prerequisite to improve device efficiency. To address this problem, the strategy of doping foreign ions into $CsPbBr_3$ perovskite lattice has been widely investigated. Through partially replacing Cs^+ at the A-site with Li^+, Na^+, K^+ and Rb^+, the grain sizes of $CsPbI_2Br$ and $CsPbBr_3$ films can be increased to reduce charge recombination [15, 18]. In addition to the substitution at A-site, replacing partial Pb^{2+} at B-site with metal ions of the same or different valences can also have a passivation effect on the perovskite grains. Moreover, In^{3+}, Al^{3+}, Ca^{2+}, Cd^{2+}, Sr^{2+}, Sn^{2+}, Sm^{3+}, Tb^{3+}, Ho^{3+}, Er^{3+} and Yb^{3+} in $MAPbI_3$ and $CsPbBr_3$ are respectively used to replace Pb^{2+}, which increases grain size and reduces non-radiative recombination rate [19 – 24]. Compared with isovalent substitution, heterovalent substitution can easily result in the formation of defect states [19, 25]. So far, there have been no reports on the effects of doping iodine ion on the structure and optoelectronic properties of $CsPbBr_3$ layer, as well as the photovoltaic property of corresponding devices.

In this study, doping PbI_2 can regulate the crystallinity of all-inorganic $CsPbBr_3$ film. Meanwhile, the $CsPbBr_3$ layer prepared by doping PbI_2 has a lower optical band gap, indicating the absorption of more solar light. In addition, the carrier recombination probability of the $CsPbBr_3$ layer is reduced after doping PbI_2. More importantly, the $CsPbBr_3$ cell based on PbI_2 achieves a champion efficiency of 6.46 %, which is much higher than 5.00 % for the undoped $CsPbBr_3$ cell. These findings suggest that doping PbI_2 offers a novel strategy for improving the quality of perovskite and the photovoltaic performance of all-inorganic $CsPbBr_3$ devices.

2. EXPERIMENTAL DETAILS

2.1. Device preparation

Before manufacturing solar cells, FTO glass was thoroughly ultrasonically rinsed with acetone, isopropanol, ethanol and deionized water. A uniform and dense Nb_2O_5

* Corresponding author: F. Zhao
E-mail: *zhaofei@czu.cn*

film was prepared on a clean FTO glass substrate by magnetron sputtering technology. The detailed information is as follows. The vacuum degree and substrate temperature for preparing Nb_2O_5 films are 3×10^{-4}Pa and 25 °C, respectively. The power and time used for sputtering Nb_2O_5 are 130 W and 40 min, severally. The undoped $CsPbBr_3$ layer was manufactured via a multi-step solution deposition method. 1 M $PbBr_2$ solution in N,N-dimethylformamide (DMF) was deposited on the Nb_2O_5/FTO at 2000 rpm for 30 s. Then, the $PbBr_2$ film was heated at 90 °C for 30 min. Subsequently, 0.07 M CsBr methanol solution was deposited on the $PbBr_2/Nb_2O_5$/FTO at 2000 rpm for 30 s. Afterwards, the CsBr film was annealed at 250 °C for 5 min. The deposition and annealing times of CsBr are both 4 times. This successfully prepared an excellent $CsPbBr_3$ perovskite film. The PbI_2-doped $CsPbBr_3$ perovskite was prepared by adding a certain proportion of PbI_2 to $PbBr_2$ solution. The rest of the process is the same as the above program. Eventually, a carbon electrode containing the area of 0.09 cm^2 was prepared on the $CsPbBr_2/Nb_2O_5$/FTO through scraping carbon paste.

2.2. Characterizations

The morphology of the $CsPbBr_3$ layer was gained by employing a field-emission scanning electron microscope (SEM). The X-ray pattern of the $CsPbBr_3$ layer was recorded by utilizing an X-ray diffractometer (XRD). XPS spectroscopy can be used to analyze the elemental valence states of perovskite layers. The absorption spectra of different $CsPbBr_3$ layers were characterized to gain the optical band gaps of various $CsPbBr_3$ layers. The time-resolved PL (TRPL) spectra for $CsPbBr_3$ layers were conducted to obtain their carrier lifetimes. The photovoltaic parameters of $CsPbBr_3$ solar cells were obtained by J-V curves tested under AM 1.5 G (100 mW/cm^2).

3. RESULTS AND DISCUSSIONS

Fig. 1 a indicates the XRD patterns of different $CsPbBr_3$ films. The three typical peaks in all films appeared at 15.23°, 21.73° and 30.80°, corresponding to the (100), (110) and (200) crystal planes of the $CsPbBr_3$ [26]. In addition, there is a diffraction peak of 26.61° in both films, corresponding to FTO substrate [27]. No distinct impurity phase is found in all $CsPbBr_3$ films. For all $CsPbBr_3$ films, the diffraction peak intensity of the (110) crystal plane is higher than that of other crystal planes, indicating that the $CsPbBr_3$ films have undergone preferential growth. Meanwhile, the main peak intensity of the PbI_2-doped $CsPbBr_3$ film is higher than that of the undoped $CsPbBr_3$ films, showing the higher crystalline quality of the $CsPbBr_3$ films with doping PbI_2. Fig. 1b and c indicate the enlarged XRD spectra of (110) and (200) for the $CsPbBr_3$ without and with doping PbI_2. The (110) diffraction peak of $CsPbBr_3$ layer shifts towards lower angle with the doping of PbI_2, which attributes to the lattice expansion of perovskite induced by iodine ions [28]. Meanwhile, we found that the behavior of the (200) diffraction peak is consistent with that of the (110) diffraction peak. Fig. 1d indicates the Full Width at Half Maximum (FWHM) for (110) in different samples. Compared with the undoped $CsPbBr_3$ film, the FWHM of the PbI_2-doped $CsPbBr_3$ film is smaller. This suggests that the $CsPbBr_3$ films with doping PbI_2 have larger grain sizes.

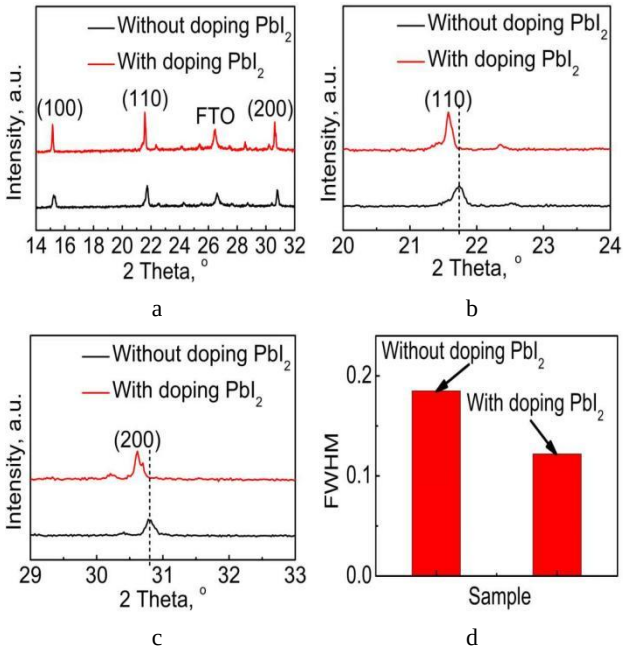

Fig. 1. a – XRD spectra of different $CsPbBr_3$ films; enlarged XRD spectra: b – (110); c – (200) for $CsPbBr_3$ without and with doping PbI_2; d – FWHM of (110) for different samples

Fig. 2 a indicates the XPS spectra (Br 3d) of various $CsPbBr_3$ films. The characteristic peak of $CsPbBr_3$ film shifts towards the direction of low binding energy after doping PbI_2, demonstrating that iodine ions have been successfully doped into the $CsPbBr_3$ lattice. This result is consistent with the XRD analysis result. Fig.2b indicates the XPS spectra (I 3d) of the PbI_2-doped $CsPbBr_3$ film. From Fig. 2 b, it can be seen that the two characteristic peaks indicate that iodine ions are already present in $CsPbBr_3$ films.

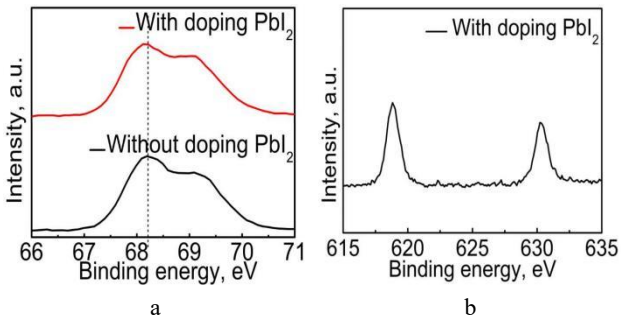

Fig. 2. a – XPS spectra (Br 3d) of various $CsPbBr_3$ films; b – XPS spectra (I 3d) of PbI_2-doped $CsPbBr_3$ film

The SEM is commonly used to study the surface morphology of $CsPbBr_3$ layer. As seen in Fig. 3, there are a relatively uneven grains on the undoped $CsPbBr_3$ films. However, more uniform grains existed on the PbI_2-doped $CsPbBr_3$ films. Clearly, the PbI_2-doped $CsPbBr_3$ layer has a larger average grain size compared with the undoped $CsPbBr_3$ layer, showing that doping PbI_2 can promote the growth of $CsPbBr_3$ films. Additionally, we also observed that the $CsPbBr_3$ layers with doping PbI_2 have fewer grain boundaries. The aforementioned results are beneficial for

improving the photovoltaic performance of $CsPbBr_3$ cells [29].

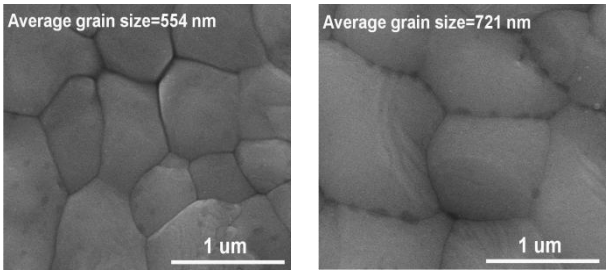

a b

Fig. 3. Surface SEM images: a – undoped $CsPbBr_3$ film; b – PbI_2-doped $CsPbBr_3$ film

In order to investigate the optical absorption properties of different $CsPbBr_3$ layers, we conducted UV-VIS spectroscopy tests. As seen in Fig. 4, the light absorption of the PbI_2-doped $CsPbBr_3$ layer is stronger in comparison to that of the undoped $CsPbBr_3$ layer. The absorption enhancement may be attributed to the high crystallinity based on few grain boundaries for the PbI_2-doped $CsPbBr_3$ layer [30, 31]. In addition, the absorption edge of PbI_2-doped device exhibits a red shift phenomenon compared with undoped devices. This indicates that the optical band gap of PbI_2-doped devices is smaller. The above analysis results suggest that doping PbI_2 reduces the optical band gap of $CsPbBr_3$ layer. The reduction of the band gap can facilitate the more absorption of the photons for $CsPbBr_3$ cells, thereby generating many electron-hole pairs within the device. Ultimately, this effectively improves the short-circuit current density of the $CsPbBr_3$ device.

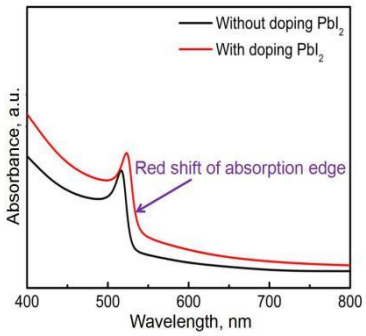

Fig. 4. Absorption spectra of undoped $CsPbBr_3$ film and PbI_2-doped $CsPbBr_3$ film

As shown in Fig. 5, TRPL measurements for different $CsPbBr_3$ samples grown on FTO substrates were conducted to investigate carrier dynamics and carrier lifetime. The carrier lifetime can be well obtained by Eq. 1:

$$f(t) = A_1 exp(\frac{-t}{\tau_1}) + A_2 exp(\frac{-t}{\tau_2}) + B, \quad (1)$$

where τ_1 and τ_2 reflect the slow and fast decay time constants, whilst A_1, A_2 are the fractional amplitudes of τ_1 and τ_2, separately. The average carrier lifetime (τ_{ave}) can be calculated to ascertain the entire recombination process, as shown by Eq. 2:

$$\tau_{ave} = \frac{\sum A_i \tau_i}{\sum A_i}. \quad (2)$$

The undoped $CsPbBr_3$ layer has an τ_{ave} value of 16.48 ns whereas an obviously improved τ_{ave} value of 36.03 ns can be detected for the PbI_2-doped $CsPbBr_3$ layer. The enhancement of the τ_{ave} value reveals that the carrier recombination probability and defect density in the $CsPbBr_3$ with doping PbI_2 are lower, which contributes to the process of photo-induced carrier transport and the final cell performance [32].

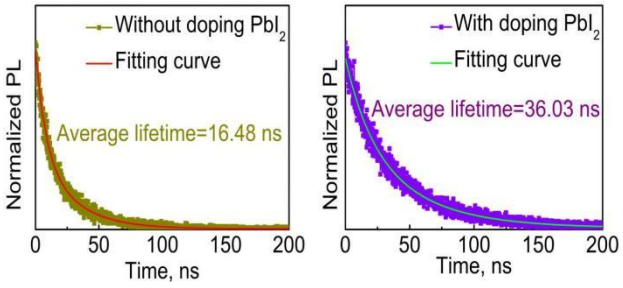

a b

Fig. 5. TRPL spectra of a – undoped $CsPbBr_3$, b – PbI_2-doped $CsPbBr_3$ films deposited on FTO substrates

To investigate the photovoltaic performance of $CsPbBr_3$ cells, we first prepared a fully structured device. Our device consists of FTO glass substrate, Nb_2O_5 electronic transport layer, $CsPbBr_3$ absorption layer and carbon electrode. It is worth noting that there is no expensive hole transport layer in our device, which greatly saves the preparation cost of the device. After preparing the complete $CsPbBr_3$ device, we conducted J-V tests on different devices. Fig. 6 a and Table 1 exhibit the J-V characteristics and corresponding photovoltaic parameters of different $CsPbBr_3$ cells, respectively.

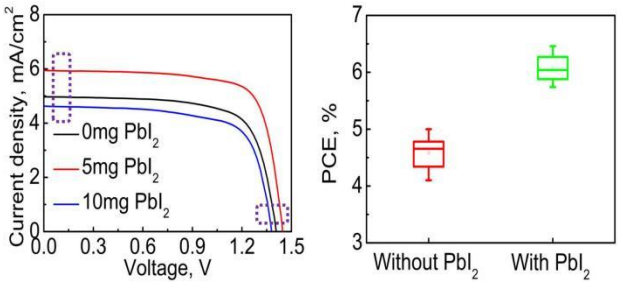

a b

Fig. 6. a – J-V curves of $CsPbBr_3$ cell with different doping amount of PbI_2; b – average efficiency of $CsPbBr_3$ cell without and with doping PbI_2

Table 1. Photovoltaic parameters of $CsPbBr_3$ cell with different doping amount of PbI_2

Samples	V_{oc}, V	J_{sc}, mA/cm^2	*FF*, %	*PCE*, %
0 mg PbI_2	1.406	4.97	71.59	5.00
5 mg PbI_2	1.445	5.94	75.22	6.46
10 mg PbI_2	1.379	4.63	70.51	4.50

The $CsPbBr_3$ cell with 0mg PbI_2 yields a relatively low efficiency of 5.00 %, coupled with an open-circuit voltage (V_{oc}) of 1.406 V, a short-circuit current density (J_{sc}) of 4.97 mA/cm^2 and a fill factor (*FF*) of 71.59 %. It is evident

that the photovoltaic performance of the solar cells with 5 mg PbI_2 outperform the unchanged devices. This marked improvement of J_{sc}, V_{oc} and *FF* can be attributed to enhanced crystallinity, reduced band gap, and decreased carrier recombination [33, 34]. The optimal incorporation of PbI_2 culminates in the champion cell, boasting an efficiency of 6.46 %, a V_{oc} of 1.445 V, a J_{sc} of 5.94 mA/cm^2, and an *FF* of 75.22 %. However, excessive incorporation of PbI_2 can reduce the photovoltaic performance of the device. Therefore, the optimal doping amount of PbI_2 is 5 mg. Fig. 6 b shows the average efficiency of the $CsPbBr_3$ cell without or with doping PbI_2. After incorporating PbI_2, the average efficiency of $CsPbBr_3$ cell (10 device) is 6.08 %, which shows the good repeatability of the device.

Fig. 7 a shows the Stability of $CsPbBr_3$ cell with doping PbI_2. The PbI_2-doped device is stored under approximately 80 % humidity and 25 °C. The PbI_2-doped device exhibits 97 % of initial efficiency, indicating superior stability of our device.

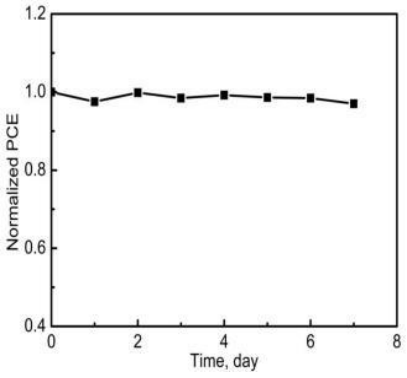

Fig. 7. Stability of $CsPbBr_3$ cell with doping PbI_2

According to previous reports [35], it has been found that iodine doping can improve the purity and phase stability of single crystal $CsPbBr_3$ films and help regulate the optical band gap. In our study, iodine doping can improve the crystallinity of polycrystalline $CsPbBr_3$ films, reduce their optical bandgap, and decrease their carrier recombination probability. More importantly, the efficiency of polycrystalline $CsPbBr_3$ solar cell has been significantly improved after iodine doping.

4. CONCLUSIONS

The PbI_2-doped all-inorganic $CsPbBr_3$ film and corresponding cell have been successfully prepared. The XRD and XPS tests indicate that iodine ions have been successfully doped into the lattice of $CsPbBr_3$ film. After PbI_2 incorporation, the crystallinity of $CsPbBr_3$ film is better and its optical band gap is smaller. Meanwhile, the PbI_2-doped $CsPbBr_3$ film possesses a less number of grain boundary defects and a lower probability of carrier recombination. Compared with the undoped $CsPbBr_3$ cell, the PbI_2-doped $CsPbBr_3$ cell achieves an outstanding efficiency of 6.46% with a V_{oc} of 1.445V, a J_{sc} of 5.94mA/cm^2 and a *FF* of 75.22%. This work provides a reasonable and effective process for the manufacturing of all-inorganic $CsPbBr_3$ cell.

Acknowledgements

This work was financed by the National Natural Science Foundation of China (No. 52402224 and No. 12304043).

REFERENCES

1. **Rong, Y., Hu, Y., Mei, A., Tan, H., Saidaminov, M.I., Seok, S.I., McGehee, M.D., Sargent, E.H., Han, H.** Challenges for Commercializing Perovskite Solar Cells *Science* 361 2018: pp. eaat8235. http://dx.doi.org/10.1126/science.aat8235
2. **Yoo, J.J., Seo, G., Chua, M.R., Park, T.G., Lu, Y., Rotermund, F., Kim, Y.K., Moon, C.S., Jeon, N.J., Correa-Baena, J.P.** Efficient Perovskite Solar Cells via Improved Carrier Management *Nature* 590 2021: pp. 587 – 593. https://doi.org/10.1038/s41586-021-03285-w
3. **Jeong, J., Kim, M., Seo, J., Lu, H., Ahlawat, P., Mishra, A., Yang, Y., Hope, M.A., Eickemeyer, F.T., Kim, M.** Pseudo-halide Anion Engineering for α-$FAPbI_3$ Perovskite Solar Cells *Nature* 592 2021: pp. 381 – 385. https://doi.org/10.1038/s41586-021-03406-5
4. **Hossain, M.I., Saleque, A.M., Ahmed, S., Saidjafarzoda, I., Shahiduzzaman, M., Qarony, W., Knipp, D., Biyikli, N., Tsang, Y.H.** Perovskite/perovskite Planar Tandem Solar Cells: A Comprehensive Guideline for Reaching Energy Conversion Efficiency Beyond 30% *Nano Energy* 79 2021: pp. 105400. https://doi.org/10.1016/j.nanoen.2020.105400
5. **Chen, J., Wu, Z., Chen, S., Zhao, W., Zhang, Y., Ye, W., Yang, R., Gong, L., Peng, Z., Chen, J.** Light Harvesting and Carrier Transfer Enhancement of All-inorganic $CsPbBr_3$ Perovskite Solar Cells by Al-doped ZnO Nanorod Arrays *Materials Science in Semiconductor Processing* 174 2024: pp. 108186. https://doi.org/10.1016/j.mssp.2024.108186
6. **Xu, Y., Yan, C., Liang, H., Huang, S., Feng, P., Song, J.** Large-scale Preparation of $CsPbBr_3$ Perovskite Quantum Dot/EVA Composite Adhesive Film by Melting for Crystal Silicon Solar Cell *Nanotechnology* 35 2024: pp. 175404. https://doi.org/10.1088/1361-6528/ad2157
7. **Dunfield, S.P., Bliss, L., Zhang, F., Luther, J.M., Zhu, K., Hest, M.F., Reese, M.O., Berry, J.J.** From Defects to Degradation: A Mechanistic Understanding of Degradation in Perovskite Solar Cell Devices and Modules *Advanced Energy Materials* 10 2020: pp. 1904054. https://doi.org/10.1002/aenm.201904054
8. **Wei, J., Wang, Q., Huo, J., Gao, F., Gan, Z., Zhao, Q., Li, H.** Mechanisms and Suppression of Photoinduced Degradation in Perovskite Solar Cells *Advanced Energy Materials* 11 2021: pp. 2002326. https://doi.org/10.1002/aenm.202002326
9. **Ouedraogo, N.A.N., Chen, Y., Xiao, Y.Y., Meng, Q., Han, C.B., Yan, H., Zhang, Y.** Stability of All-inorganic Perovskite Solar Cells *Nano Energy* 67 2020: pp. 104249. https://doi.org/10.1016/j.nanoen.2019.104249
10. **Faheem, M.B., Khan, B., Feng, C., Farooq, M.U., Raziq, F., Xiao, Y., Li, Y.** All-inorganic Perovskite Solar Cells: Energetics, Key Challenges, and Strategies toward Commercialization *ACS Energy Letters* 5

2020: pp. 290 – 320.
http://doi.org/10.1021/acsenergylett.9b02338

11. **Tian, J., Xue, Q., Yao, Q., Li, N., Brabec, C.J., Yip, H.L.** Inorganic Halide Perovskite Solar Cells: Progress and Challenges *Advanced Energy Materials* 10 2020: pp. 2000183.
https://doi.org/10.1002/aenm.202000183

12. **Yuan, B., Zhou, Y., Liu, T., Li, C., Cao, B.** Extending the Absorption Spectra and Enhancing the Charge Extraction by the Organic Bulk Heterojunction for $CsPbBr_3$ Perovskite Solar Cells *ACS Sustainable Chemistry & Engineering* 11 2023: pp. 718 – 725.
https://doi.org/10.1021/acssuschemeng.2c05859

13. **Chai, W., Zhu, W., Zhang, Z., Liu, D., Ni, Y., Song, Z., Dong, P., Chen, D., Zhang, J., Zhang, C., Hao, Y.** $CsPbBr_3$ Seeds Improve Crystallization and Energy Level Alignment for Highly Efficient $CsPbI_3$ Perovskite Solar Cells *Chemical Engineering Journal* 452 2023: pp. 139292.
https://doi.org/10.1016/j.cej.2022.139292

14. **Wang, Y., Tong, A., Wang, Y., Liang, K., Zhu, W., Wu, Y., Sun, W., Wu, J.** Interfacial Modulation by Ammonium Salts in Hole Transport Layer Free $CsPbBr_3$ Solar Cells with Fill Factor over 86 % *Materials Today Chemistry* 40 2024: pp. 102228.
https://doi.org/10.1016/j.mtchem.2024.102228

15. **Lau, C.F.J., Deng, X., Ma, Q., Zheng, J., Yun, J.S., Green, M.A., Huang, S., Ho-Baillie, A.W.Y.** $CsPbIBr_2$ Perovskite Solar Cell by Spray Assisted Deposition *ACS Energy Letters* 1 2016: pp. 573 – 577.
http://doi.org/10.1021/acsenergylett.6b00341

16. **Li, Y.N., Duan, J.L., Yuan, H.W., Zhao, Y.Y., He, B.L., Tang, Q.W.** Lattice Modulation of Alkali Metal Cations Doped $Cs_{1-x}R_xPbBr_3$ Halides for Inorganic Perovskite Solar Cells *Solar RRL* 2018: pp. 1800164.
https://doi.org/10.1002/solr.201800164

17. **Zhang, L., Zhang, X.Z., Xu, X.X., Tang, J., Wu, J.H., Lan, Z.** CH_3NH_3Br Additive for Enhanced Photovoltaic Performance and Air Stability of Planar Perovskite Solar Cells Prepared by Two-step Dipping Method *Energy Technology* 5 2017: pp. 1887 – 1894.
https://doi.org/10.1002/ente.201700561

18. **Guo, Y., Wang, Q., Saidi, W.A.** Structural Stabilities and Electronic Properties of High-angle Grain Boundaries in Perovskite Cesium Lead Halides *Journal of Physical Chemistry C* 121 2017: pp. 1715 – 1722.
https://doi.org/10.1021/acs.jpcc.6b11434

19. **Nam, J.K., Chai, S.U., Cha, W., Choi, Y.J., Kim, W., Jung, M.S., Kwon, J., Kim, D., Park, J.H.** Potassium Incorporation for Enhanced Performance and Stability of Fully Inorganic Cesium Lead Halide Perovskite Solar Cells *Nano Letters* 17 2017: pp. 2028 – 2033.
https://doi.org/10.1021/acs.nanolett.7b00050

20. **Duan, J.L., Zhao, Y.Y., Yang, X.Y., Wang, Y.D., He, B.L., Tang, Q.W.** Lanthanide Ions Doped $CsPbBr_3$ Halides for HTM-free 10.14%-efficiency Inorganic Perovskite Solar Cell with An Ultrahigh Open-circuit Voltage of 1.594V *Advanced Energy Materials* 8 2018: pp. 1802346.
https://doi.org/10.1002/aenm.201802346

21. **Wang, Z.K., Li, M., Yang, Y.G., Hu, Y., Ma, H., Gao, X.Y., Liao, L.S.** High Efficiency Pb-In Binary Metal Perovskite Solar Cells *Advanced Materials* 28 2016: pp. 6695 – 6703.
https://doi.org/10.1002/adma.201600626

22. **Wang, J.T.W., Wang, Z., Pathak, S., Zhang, W., deQuilettes, D.W., Rivarola, F.W.R., Huang, J., Nayak, P.K., Patel, J.B., Yusof, H.A.M., Vaynzof, Y., Zhu, R., Ramirez, G., Zhang, J., Ducati, C., Grovenor, C., Johnston, M.B., Ginger, D.S., Nicholas, R.J., Snaith, H.J.** An Efficient Perovskite Solar Cells by Metal Ion *Energy & Environmental Science* 9 2016: pp. 2892 – 2901.
https://doi.org/10.1039/C6EE01969B

23. **Swarnkar, A., Mir, W.J., Nag, A.** Can B-Site Doping or Alloying Improve Thermal and Phase Stability of All-inorganic $CsPbX_3$ (X = Cl, Br, I) Perovskites *ACS Energy Letters* 3 2018: pp. 286 – 289.
https://doi.org/10.1021/acsenergylett.7b01197

24. **Guo, H., Pei, Y., Zhang, J., Cai, C., Zhou, K., Zhu, Y.** Doping with $SnBr_2$ in $CsPbBr_3$ to Enhance the Efficiency of All-inorganic Perovskite Solar Cells *Journal of Materials Chemistry C* 7 2019: pp. 11234 – 11243.
https://doi.org/10.1039/C9TC03359A

25. **Zou, S., Liu, Y., Li, J., Liu, C., Feng, R., Jiang, F., Li, Y., Song, J., Zeng, H., Hong, M., Chen, X.** Stabilizing Cesium Lead Halide Perovskite Lattice Through Mn(II) Substitution for Air-stable Light-emitting Diodes *Journal of the American Chemical Society* 139 2017: pp. 11443 – 11450.
https://doi.org/10.1021/jacs.7b04000

26. **Zhang, Z., Zhu, W., Han, T., Wang, T., Chai, W., Zhu, J., Xi, H., Chen, D., Lu, G., Dong, P., Zhang, J., Zhang, C., Hao, Y.** Accelerated Sequential Deposition Reaction via Crystal Orientation Engineering for Low-temperature, High-efficiency Carbon-electrode $CsPbBr_3$ Solar Cells *Energy & Environmental Materials* 7 2024: pp. e12524.
https://doi.org/10.1002/eem2.12524

27. **Sun, H., Yu, L., Yuan, H., Zhang, J., Gan, X., Hu, Z., Zhu, Y.** $CoCl_2$ as Film Morphology Controller for Efficient Planar $CsPbIBr_2$ Perovskite Solar Cells *Electrochimica Acta* 349 2020: pp. 136162.
https://doi.org/10.1016/j.electacta.2020.136162

28. **Atourki, L., Vega, E., Mollar, M., Kirou, H., Bouabid, K., Ihlal, A.** Impact of Iodide Substitution on the Physical Properties and Stability of Cesium Lead Halide Perovskite Thin Films $CsPbBr_{3-x}I_x$ ($0 \leq x \leq 1$) *Journal of Alloys and Compounds* 702 2017: pp. 404 – 409.
http://dx.doi.org/10.1016/j.jallcom.2017.01.205

29. **Liu, X., Tan, X., Liu, Z., Ye, H., Sun, B., Shi, T., Tang, Z., Liao, G.** Boosting the Efficiency of Carbon-based Planar $CsPbBr_3$ Perovskite Solar Cells by a Modified Multistep Spin-coating Technique and Interface Engineering *Nano Energy* 56 2019: pp. 184 – 195.
https://doi.org/10.1016/j.nanoen.2018.11.053

30. **Zhu, W., Bao, C., Wang, Y., Li, F., Zhou, X., Yang, J., Lv, B., Wang, X., Yu, T., Zou, Z.** Coarsening of One-step Deposited Organolead Triiodide Perovskite Films via Ostwald Ripening for High Efficiency Planar-heterojunction Solar Cells *Dalton Transactions* 45 2016: pp. 7856 – 7865.
https://doi.org/10.1039/C6DT00900J

31. **Zhao, F., Guo, Y., Tao, J., Li, Z., Jiang, J., Chu, J.** Investigation of $CsPbBr_3$ Films with Controllable Morphology and Its Influence on the Photovoltaic Properties for Carbon-based Planar Perovskite Solar Cells *Applied Optics* 59 2020: pp. 5481 – 5486.
https://doi.org/10.1364/AO.392404

32. **Zhou, L., Sui, M., Zhang, J., Cao, K., Wang, H., Yuan, H., Lin, Z., Zhang, J., Li, P., Hao, Y., Chang, J.** Tailored Buried Layer Passivation toward High-efficiency Carbon Based All-inorganic $CsPbBr_3$ Perovskite Solar Cell

Chemical Engineering Journal 496 2024: pp. 154043. https://doi.org/10.1016/j.cej.2024.154043

33. **Zhao, Y., Wang, Y., Duan, J., Yang, X., Tang, Q.** Divalent Hard Lewis Acid Doped $CsPbBr_3$ Films for 9.63%-efficiency and Ultra-stable All-inorganic Perovskite Solar Cells *Journal of Materials Chemistry A* 7 2019: pp. 6877 – 6882. https://doi.org/10.1039/C9TA00761J

34. **Jiang, X., Geng, C., Yu, X., Pan, J., Zheng, H., Liang, C., Li, B., Long, F., Han, L., Cheng, Y., Peng, Y.** Doping with KBr to Achieve High-performance $CsPbBr_3$ Semitransparent Perovskite Solar Cells *ACS Applied Materials & Interfaces* 16 2024: pp. 19039 – 19047. https://doi.org/10.1021/acsami.4c02402

35. **Sujith, P., Parne, S., Predeep, P.** Iodine Doping of $CsPbBr_3$: Toward Highly Stable and Clean Perovskite Single Crystals for Optoelectronic Applications *Philosophical Magazine* 103 2023: pp. 1213 – 1231. https://doi.org/10.1080/14786435.2023.21957